Eur. Phys. J. C (2024) 84:815
https://doi.org/10.1140/epjc/s10052-024-13182-x

THE EUROPEAN PHYSICAL JOURNAL C

Regular Article - Theoretical Physics

Variance-based uncertainty relations and entanglement amplification for particles constrained on a torus

Asma Bashir[1,a], **Hafiz Muhammad Asif Javed**[1,b], **Muhammad Abdul Wasay**[3,c], **Muhammad Shabir Mahr**[1,d], **Muhammad Zafar Iqbal**[2]

[1] Department of Physics, University of Agriculture, Faisalabad 38040, Pakistan
[2] Department of Mathematics and Statistics, University of Agriculture, Faisalabad 38040, Pakistan
[3] School of Theoretical Physics, Hunan University, Changsha 410082, China

Received: 19 May 2024 / Accepted: 29 July 2024

Abstract We formulate the variance-based uncertainty relations (URs) via the Robertson's inequality, for a 2-particle entangled system constrained on a torus and subject to a stationary magnetic field $\vec{\mathcal{B}}$. We explore the system's parameter space and show that these new URs have field-tunable uncertainty bounds. Our analysis reveals that $\vec{\mathcal{A}}$ (vector potential) induces a phase shift in the state, due to the Aharonov–Bohm effect, leading to a perturbed system dynamics which results in asymmetric product of variance ($\mathcal{POV}$). Additionally, we give the critical range of $\vec{\mathcal{A}}$ and $\vec{\mathcal{B}}$ where the system acts as an entanglement amplifier; this amplification is also discussed under various geometric parameters. The possibility of reducing the $\mathcal{POV}$ of the conjugate pair $[q, p]$ below the known benchmark value by the Generalized Uncertainty Relation (GUR) is also demonstrated. Finally, we check the susceptibility of state coherence to $\vec{\mathcal{B}}$ by saturating the angular momentum uncertainty relation and identify the critical coherence value $\mathcal{B}_c$ such that when $\mathcal{B} \neq \mathcal{B}_c$, the state decoheres.

1 Introduction

Quantum entanglement and uncertainty relations (URs) are among the most captivating aspects of quantum mechanics and are key distinctions between the classical and quantum physics. The URs are of crucial significance in many quantum information processing applications and there has been significant advancement in this direction; e.g., see Refs. [1–3]. The UR was first introduced by Heisenberg [4] and later it was generalized by Robertson for any pair of non-commuting observables [5] which sets a bound on the precision of simultaneous measurement of these observables. The seminal work of Einstein, Podolsky and Rosen EPR – in their argument against the completeness of quantum theory – demonstrated that for a system of two correlated particles if one could precisely measure the physical quantities of one particle then the corresponding physical quantities of the second particle can be measured with *certainty* irrespective of the distance between them [6]. Hence uncertainty and entanglement are strongly linked and uncertainty for entangled systems has been extensively studied in the form of product of variance $\mathcal{POV}$, sum of variance $\mathcal{SOV}$ and entropy; see Refs. [7–10]. A similar work in this direction was done in Refs. [11,12] which provides a variance based Generalized Uncertainty Relation (GUR) for a system of entangled particles with higher measurement precision compared with the standard Heisenberg uncertainty relation (HUR). Thus uncertainty can be reduced in the presence of entanglement and it becomes possible to amplify the entanglement strength which finds many potential applications in quantum information and computing [13,14]. It is interesting to probe this idea for a system of particles constrained on curved geometries. Physics constrained on torus geometry has remained a test bed for various interesting phenomena, for instance, Ref. [15] investigated the effect of the shape of the universe on the particle dynamics assuming the topology of the universe to be a torus. It also acts as a constrained space of the equimodular states, improving the fidelity of teleported states which is a crucial element in superdense teleportation [16]. Moreover, an external magnetic field can be applied to investigate the phenomenon of Aharonov–Bohm effect in toroidal geometry [17,18]. Therefore, it seems interesting to explore

[a] e-mail: kbasmabashir807@gmail.com (corresponding author)
[b] e-mail: m.asif.javed@uaf.edu.pk
[c] e-mail: wasay31@gmail.com
[d] e-mail: shabir.mahr@uaf.edu.pk

Published online: 14 August 2024

variance based URs for a constrained and entangled system (on a torus) under the effect of a stationary external field $\vec{\mathcal{B}}$ and we address this question in this paper.

Dirac's method for identifying system dynamics given the second-class constraints has attracted attention since the inception of the idea [19] and is reported extensively for various background geometries, e.g., see Refs. [20–26]. Dirac's approach for particles constrained on geometric backgrounds is of interest because it gives access to a parameter space of the system's variables which allows parameter tuning as well as the uncertainty bounds for any pair of observables can be obtained as a function of these system variables. In this paper, we consider a system of two entangled particles constrained on the surface of torus under a stationary external magnetic field $\vec{\mathcal{B}}$. For this system, the constrained classical dynamics of the particles is obtained using Dirac's approach where the standard Poisson brackets of the classical mechanics are replaced by the Dirac brackets which contain some additional terms [19]. These terms are attributed to the particular background geometry which constrains the particles and yields new physics. These brackets result in URs upon canonical quantization (CQ) which can be cast into the $\mathcal{POV}$ form via the Robertson inequality by assuming that the two particles share an entangled state of the form given in [27,28]. The authors of [23,26] found that it is not possible to perform the CQ within intrinsic geometry, so in view of these findings we assume the embedding of the torus into a flat space of dimensions $\mathcal{D} = \mathcal{D}_I + 1$, where $\mathcal{D}_I$ represents the dimensions of intrinsic geometry.

This paper first introduces new variance based URs in the form of $\mathcal{POV}$ and then explores the parameter regimes which are favorable for lowering the $\mathcal{POV}$ in order to amplify the entanglement strength. Further details on the comparison between $\mathcal{POV}$ of these new URs with the GUR are discussed. The susceptibility of state coherence to $\vec{\mathcal{B}}$ and the phase shift induced by the Aharonov–Bohm effect for this geometric framework, is also discussed.

The paper is organized as follows: Sect. 2 presents the constrained classical dynamics of a 2-particle system using Dirac's approach. In Sect. 3, we quantize the system and discuss $\mathcal{POV}$ as a function of system parameters in view of entanglement amplification. In Sect. 4, we discuss state coherence and other aspects. Results are summarized in Sect. 5.

2 Constrained classical dynamics of 2-particle system

First we will explore the classical dynamics of the system. The torus geometry is captured by the following equation

$$\begin{pmatrix} x \\ y \\ z \end{pmatrix} = \begin{pmatrix} (a + bsin\theta)cos\phi \\ (a + bsin\theta)sin\phi \\ bcos\theta \end{pmatrix} \tag{1}$$

where, a and b are the two radii (major and minor radii, respectively) of the torus, θ and ϕ are the poloidal and toroidal angles, respectively [26]. The system consists of two particles constrained on the surface of a torus under the effect of a stationary external magnetic field $\vec{\mathcal{B}}$ applied parallel to z-axis. The Lagrangian $\mathcal{L}$ of this system can be written using Lagrange multipliers as follows:

$$\mathcal{L} = \sum_i \Bigg[\frac{1}{2} M \dot{\eta}_i^2 + e\dot{\eta}_i . \mathcal{A}_{\eta_i}(\vec{\eta}, t) - \lambda \left(a^2 - b^2 + (x_i^2 + y_i^2 + z_i^2) - 2a\sqrt{x_i^2 + y_i^2} \right) \Bigg] \tag{2}$$

where, the term inside the parenthesis represents the constraint which imposes the constraint on particle dynamics. In Eq. (2) $i = 1, 2$ is the particle index, $\dot{\eta}_i^2 = \dot{\eta}_1^2 + \dot{\eta}_2^2 = \dot{x}_1^2 + \dot{y}_1^2 + \dot{x}_2^2 + \dot{y}_2^2 + \dot{z}_1^2 + \dot{z}_2^2$, $\mathcal{A}$ is the vector potential, λ is the Lagrange multiplier (treated as a degree of freedom), e and M are the charge and mass of the particle, respectively. The Hamiltonian $\mathcal{H}$ of this system is given by the following equation,

$$\mathcal{H} = \sum_i \Bigg[p_\lambda \dot{\lambda} + \frac{1}{2M}(p_{\eta_i} - e\mathcal{A}_{\eta_i})^2 + \lambda \left(a^2 - b^2 + (x_i^2 + y_i^2 + z_i^2) - 2a\sqrt{x_i^2 + y_i^2} \right) \Bigg] \tag{3}$$

It is to be noted that the Legendre transform from $\mathcal{L}$ to $\mathcal{H}$ contains velocities $\dot{\lambda}$ and therefore the dynamics of the system can not be obtained via the standard Poisson algebra. Instead, we need Dirac's approach to obtain the correct constrained classical dynamics. For this, the primary constraint (obtained from $\mathcal{L}$, i.e., $\rho_1 = p_\lambda \approx 0$) is incorporated into $\mathcal{H}$ with the help of u (a function of time) and the resulting total Hamiltonian is then given by the following equation [19,21]:

$$\mathcal{H}_T = \sum_i \Bigg[\frac{1}{2M}(p_{\eta_i} - e\mathcal{A}_{\eta_i})^2 + \lambda \left(a^2 - b^2 + (x_i^2 + y_i^2 + z_i^2) - 2a\sqrt{x_i^2 + y_i^2} \right) + up_\lambda \Bigg] \tag{4}$$

where, $\dot{\lambda}$ is absorbed into u. Following Dirac's approach, a series of secondary constraints are also obtained by using the consistency condition which are listed below (Note, i is the summation index but $\sum_i$ is dropped for convenience hereafter).

$$\rho_2 = -\left(a^2 - b^2 + (x_i^2 + y_i^2 + z_i^2) - 2a\sqrt{x_i^2 + y_i^2}\right) \approx 0 \tag{5}$$

$$\rho_3 = -\frac{2\left[(p_{\eta_i} - e\mathcal{A}_{\eta_i}).\eta_i\sqrt{x_i^2 + y_i^2} - a\left((p_{x_i} - e\mathcal{A}_{x_i})x_i + (p_{y_i} - e\mathcal{A}_{y_i})y_i\right)\right]}{M\sqrt{x_i^2 + y_i^2}} \approx 0 \tag{6}$$

$$\rho_4 = \frac{-2(p_{\eta_i} - e\mathcal{A}_{\eta_i})^2}{M^2} + \frac{4\lambda\left(a^2 - 2a\sqrt{x_i^2 + y_i^2} + \eta_i^2\right)}{M} + \frac{2a((p_{y_i} - e\mathcal{A}_{y_i})x_i + (p_{x_i} - e\mathcal{A}_{x_i})y_i)^2}{M^2(x_i^2 + y_i^2)^{3/2}} \approx 0 \tag{7}$$

Using $\rho_1 = \rho_2 = 0$, the total Hamilton in Eq. (4) can be cast into the following form,

$$\mathcal{H}_T = \frac{1}{2M}(p_{\eta_i} - e\mathcal{A}_{\eta_i})^2 \tag{8}$$

The classical dynamics is obtained by evaluating the Dirac brackets and the elements of the inverse matrix ($\mathcal{IM}$) are given below [19,21]:

$$\mathcal{IM} = \begin{pmatrix} 0 & Q_{12}^{-1} & Q_{13}^{-1} & q \\ -Q_{12}^{-1} & 0 & -q & 0 \\ Q_{31}^{-1} & q & 0 & 0 \\ -q & 0 & 0 & 0 \end{pmatrix} \tag{9}$$

where,

$$q = \frac{M}{4\left(a^2 - 2a\sqrt{x_i^2 + y_i^2} + x_i^2 + y_i^2 + z_i^2\right)} = \frac{M}{4b^2}; \quad Q_{13}^{-1} = Q_{31}^{-1} = 0 \tag{10}$$

and

$$Q_{12}^{-1} = \frac{(3a^2 - 7a\sqrt{x_i^2 + y_i^2})\left[(p_{y_i} - e\mathcal{A}_{y_i})x_i - (p_{x_i} - e\mathcal{A}_{x_i})y_i\right]^2 + 4(x_i^2 + y_i^2)^2(p_{\eta_i} - e\mathcal{A}_{\eta_i})^2}{4Mb^4(x_i^2 + y_i^2)^2} \tag{11}$$

The Dirac brackets which entail system dynamics are given in the Appendix 6.1.

Equations (27)–(29) (see Appendix 6.1) are the Dirac brackets between position and momentum degrees of freedom of the same particle. In contrast to the Poisson algebra, the presence of the additional term $\left(\text{i.e., } x_k^2(a - \sqrt{x_i^2 + y_i^2})^2/b^2(x_i^2 + y_i^2)\right)$ in Eq. (27) (see Appendix 6.1) indicates that p_{x_k} does not generate the translations of particle-k along x-axis. This term can be written using Eq. (5) as $\left(\frac{x_k^2[2a^2 - (a^2 - b^2 + x_i^2 + y_i^2 + z_i^2)]^2}{4a^2b^2(x_i^2 + y_i^2)}\right)$, where $k = \{1, 2\}$, and it gives the extent of deviation of the particle trajectory from x-axis.

Moreover, the parameters (x, y, z) and the two radii (i.e., a, b) indicate a point on the surface of torus in 3D-Cartesian space (see Eq. (1)). hence, momentum seems to generate ranslation along a twisted (curved) path; same for the y and z-components (i.e., Eqs. (28)–(29), see Appendix).

Equations (30)–(44) (Appendix 6.1) gives the Dirac brackets between the degrees of freedom of the two distinct particles. This set of equations is in contrast with the standard Poisson algebra where all these brackets vanish. This is evident from the expression on the right side of Eqs. (30)–(44) which appears due to the constraint incorporated into the dynamics. This reveals that momentum can generate translations orthogonal to the position of the particle. Moreover, one can write the terms appearing in the expression of Eqs. (30)–(44) (see Appendix 6.1) using Eq. 5 as: $z_1 = \sqrt{\left(b^2 - a^2 - (x_i^2 + y_i^2 + z_2^2) + 2a\sqrt{x_i^2 + y_i^2}\right)}$ and $\sqrt{x_i^2 + y_i^2} = \frac{a^2 - b^2 + (x_i^2 + y_i^2 + z_i^2)}{2a}$ which involve all three position coordinates (x, y, z) and the two radii (i.e., a, b).

Equations (45)–(46) (Appendix 6.1) involves the Dirac brackets between different position degrees of freedom (which are generator of translation in the p-space (momentum space) of the particles. This set of equations is not affected by the background constraining geometry. This is because no constraint is imposed on the momentum of the particles and no ρ_i is obtained as a function of p only, which enables a full p-space access. Therefore, this set of Dirac brackets is not affected by the constraint and it coincides with the standard Poisson brackets of classical mechanics.

Equations (47)–(61) (Appendix 6.1) contains the Dirac brackets between different momentum degrees of freedom of the particles. These equations also involve the two radii and the parameters (x, y, z) and by the same argument as above, it can be concluded that the dynamics is confined to a torus and therefore momentum can generate translation

orthogonal to its initial direction of motion. Further, this set of Dirac brackets can be written using the angular momentum operator and it will be discussed in the next section.

Note that Eqs. (30)–(44) and Eqs. (47)–(61) are derived by assuming $M\sqrt{x_i^2+y_i^2}$ (in the denominator of Eq. (6)) as a constant. One can write this expression as: $M\sqrt{x_i^2+y_i^2} = \frac{I}{a} - \frac{13}{6}Mb + \frac{M\eta_i^2}{2a}$, where $I = Ma^2 + \frac{3}{2}Mb^2$ denotes the rotational inertia of a hollow torus [29] and $\eta_i^2 = x_i^2 + y_i^2 + z_i^2 = x_1^2+y_1^2+z_1^2+x_2^2+y_2^2+z_2^2$. Further, we assume (x, y, z) to vary in such a manner that η_i^2 remains fixed. Hence, this expression becomes constant and can be factored out from the derivatives while computing the Dirac brackets.

3 Dirac quantization and $\mathcal{POV}$ in the presence of entanglement

The quantum side is studied by assuming the two particles as two maximally entangled parties (subsystems), A and B. The subsystem A and B spans the Hilbert space $\mathcal{H}_A$ and $\mathcal{H}_B$, respectively, with the global state of the bipartite system spanning $\mathcal{H}_C = \mathcal{H}_A \otimes \mathcal{H}_B$. Since, we assume a 2-particle constrained classical system which is partitioned into two subsystems, each subsystem contains only one particle and each particle acts as a subsystem of the global system. The state of the composite system of these entangled particles is written as follows [27,28]:

$$\Psi(\theta,\phi) = \alpha\xi_1(\theta_1,\phi_1)\chi_1(\theta_2,\phi_2) + \beta\xi_2(\theta_1,\phi_1)\chi_2(\theta_2,\phi_2) \tag{12}$$

where $|\alpha|^2 + |\beta|^2 = 1$, and ξ and χ represent the basis vectors of A and B, respectively. Due to the rotational symmetry around z-axis, one can write the basis vectors of each subsystem using one-particle state on the surface of torus as [30,31]:

$$\xi(\theta,\phi) = \exp(im\phi)\psi(\theta) \tag{13}$$

where m is an integer. Further, one can write the function $\psi(\theta)$ as: $\psi = b\exp(i\theta)$. Hence, the global state of the system can be written using Eq. (13) and the polar form of $\psi(\theta)$ in Eq. (12) as follows:

$$\Psi(\theta,\phi) = \sqrt{2}b^2 e^{i[m(\phi_i+\phi_1\phi_2)+(\theta_i+\theta_1\theta_2)]} \tag{14}$$

Assuming a torus with aspect ratio $a/b = 3$, one obtains the expression for b as follows:

$$b_+ = \frac{1}{2}\sqrt{x_i^2+y_i^2} - \frac{z_i^2}{2\sqrt{x_i^2+y_i^2}} \tag{15}$$

$$b_- = \frac{1}{4}\sqrt{x_i^2+y_i^2} + \frac{z_i^2}{2\sqrt{x_i^2+y_i^2}} \tag{16}$$

We will use b_+ as b in the rest of the paper. The quantum dynamics is obtained via the Dirac quantization rule: $\frac{\{\,,\,\}_{DB}}{i\hbar} \to [\,,\,]$ with $\hbar = 1$. The resulting URs are cast into the $\mathcal{POV}$ form (see Appendix 6.2), using the Robertson inequality, to compute the uncertainty bounds achievable for a pair of observables of the constrained quantum system. In the following sections, we will probe $\mathcal{POV}$s in connection to controllable entanglement strengths via system parameters.

3.1 Correlation between observables

The graphs in the following sections are plotted for the parameter values: $x_1 = 2$, $x_2 = 3.1$, $y_1 = 2.45$, $y_2 = 0.65$, $k = 2$, $\mathcal{A} = 0.5$, $m = 1$, $\alpha = 4$, $\hbar = 1$, $e = 1$, $z_1 = 2$, $z_2 = 1$. The poloidal and toroidal angles (in radians) are specified by Eq. (85) (see Appendix 6.2).

The scatter plot matrix in Fig. 1 provides a visualization of the mutual dependence/independence of the degrees of freedom of distinct subsystems, which is useful for testing degree of correlation between observables of different subsystems. Eigenvalues are computed for the entangled state given by (14).

Note that the derivative operators in the eigenvalue equation ($\hat{p}\Psi(\theta,\phi) = -i\hbar\nabla\Psi(\theta,\phi)$), for toroidal geometry, are given in Eqs. (86)–(88) (see Appendix 6.2)). The momentum eigenvalues for the x and y components are given below:

$$\hat{p}_{x_1}\Psi(\theta,\phi) = \left[-\frac{m\hbar\sin\phi_1(1+\phi_2)}{(a+b\sin\theta_1)} - \frac{x_1\hbar\cos\theta_1(1+\theta_2)(a-\sqrt{x_i^2+y_i^2})}{b^2\sin\theta_1\sqrt{x_i^2+y_i^2}} \right]\Psi(\theta,\phi) \tag{17}$$

$$\hat{p}_{y_1}\Psi(\theta,\phi) = \left[\frac{m\hbar\cos\phi_1(1+\phi_2)}{(a+b\sin\theta_1)} - \frac{y_1\hbar\cos\theta_1(1+\theta_2)(a-\sqrt{x_i^2+y_i^2})}{b^2\sin\theta_1\sqrt{x_i^2+y_i^2}} \right]\Psi(\theta,\phi) \tag{18}$$

$$\hat{p}_{x_2}\Psi(\theta,\phi) = \left[-\frac{m\hbar\sin\phi_2(1+\phi_1)}{(a+b\sin\theta_2)} - \frac{x_2\hbar\cos\theta_2(1+\theta_1)(a-\sqrt{x_i^2+y_i^2})}{b^2\sin\theta_2\sqrt{x_i^2+y_i^2}} \right]\Psi(\theta,\phi) \tag{19}$$

$$\hat{p}_{y_2}\Psi(\theta,\phi) = \left[\frac{m\hbar\cos\phi_2(1+\phi_1)}{(a+b\sin\theta_2)} \right.$$

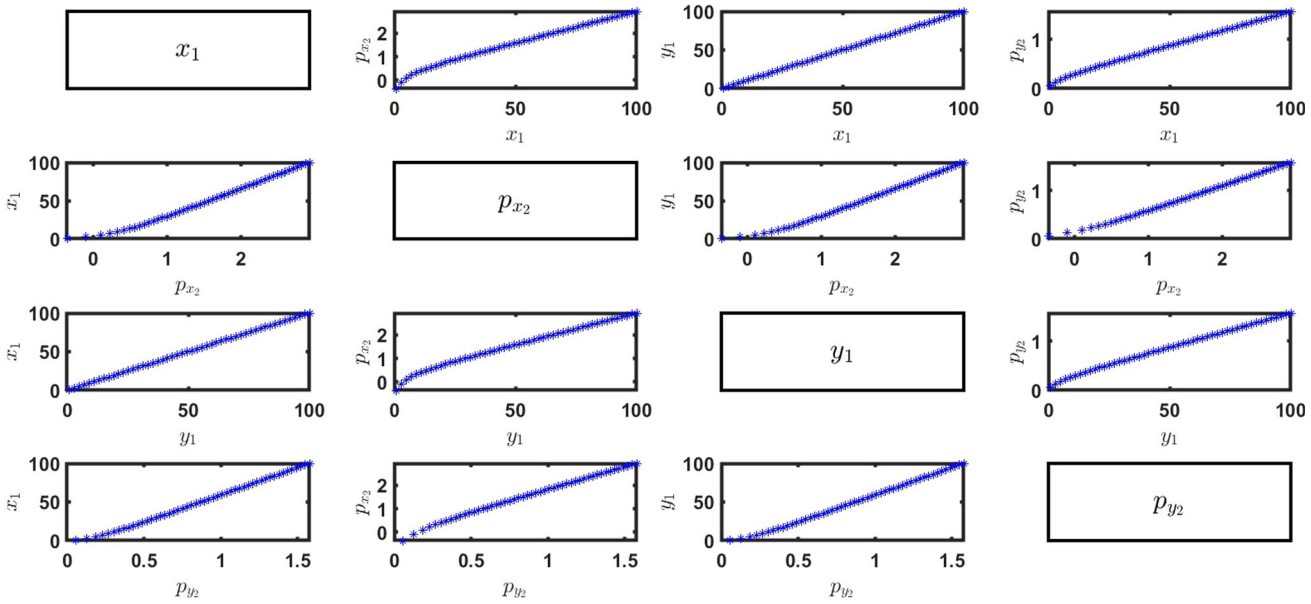

Fig. 1 Scatter plot matrix representing correlation between degrees of freedom of different subsystems. The eigenvalues of position and momentum observables of different subsystems are analysed to check the mutual dependence of the degrees of freedom of the two particles. The graphs are plotted for $x_1 = y_1 = [0, 100]$, $\theta_1 = \phi_1 = [0, 2\pi]$, $b = 2$. All other parameter values same as described above

$$-\frac{y_2\hbar\cos\theta_2(1+\theta_1)(a-\sqrt{x_i^2+y_i^2})}{b^2\sin\theta_2\sqrt{x_i^2+y_i^2}}\Bigg]\Psi(\theta,\phi) \qquad (20)$$

Each subplot in Fig. 1 is a scatter plot for different combinations of the position and momentum observables and the variable mentioned on the diagonal defines the horizontal (vertical) axis of each scatter plot of that row (column). It is evident that there exists a positive correlation between all the degrees of freedom. This is due to the presence of the term on the right side of the $\mathcal{POV}$ in Eqs. (65)–(84) (see Appendix 6.2) which arises due to the constraint, resulting in a mutual dependence of these observables. Additionally, since the particles share an entangled state (i.e., Eq. (14)), the eigenvalues exhibit strong correlation between the observables of the two subsystems. Hence, the geometry of torus and the bipartite entanglement is responsible for the mutual dependence of the observables of each subsystem. Thus, the dynamics of one subsystem is strongly influenced by the simultaneous position of the other subsystem. Results in Fig. 1 are obtained for a fixed value of the minor radius i.e., $b = 2$. However, increasing (x, y, z) increases a (see Eq. 5), resulting in a geometrically expanding ring-shaped torus with $a >> b$. The subplots in the first and third row of Fig. 1 exhibit the effect of this geometric expansion on the correlation between observables. One can see a nonlinear correlation (for particles very close to origin) followed by a linear positive correlation as the particles distance from origin increases. This is because the particles near the origin are closer to the z-axis (and hence $\vec{\mathcal{B}}$) and the interaction of the particles with the field results in dissipation of the entanglement, leading to nonlinear-like trend. However, when the particles are away from origin (i.e., $\vec{\mathcal{B}}$), the entanglement restores and the degrees of freedom of both particles are linearly correlated as observed in *entanglement revival* [32]. Additionally, one can see, this correlation sustains even for increasing particle distance, representing *long-distance* bipartite entanglement [33]. The same is observed for all the scatter plots of Fig. 1 representing correlation between different momentum observables. The subplots for the relationship between position observables exhibit a perfect linear positive correlation regardless of the particle distance from origin. This is because although the position observables commute (see Eqs. 45–46 in Appendix 6.1) and are mutually independent, the correlation in the scatter plot represent the quantum correlation due to the presence of entanglement. These results suggest that any change in the position of one particle will induce an equal change in position of the other particle.

Although this matrix plot illustrates the covariance of the degrees of freedom of the two subsystems, it seems more insightful to check how one can control the $\mathcal{POV}$ between the observables in the presence of these correlations. To achieve this, we compute the $\mathcal{POV}$ via the Robertson relation and provide a measure of the entanglement strength via quantification of the uncertainty between the observables. The uncertainty relations are obtained via Dirac quantization of the brackets given in Appendix 6.1. While computing the $\mathcal{POV}$ for the commutators corresponding to Eqs. (47)–(48) (see Appendix 6.1), $(x_k p_{y_k} - y_k p_{x_k})$ can be written as $L_z^{(k)}$

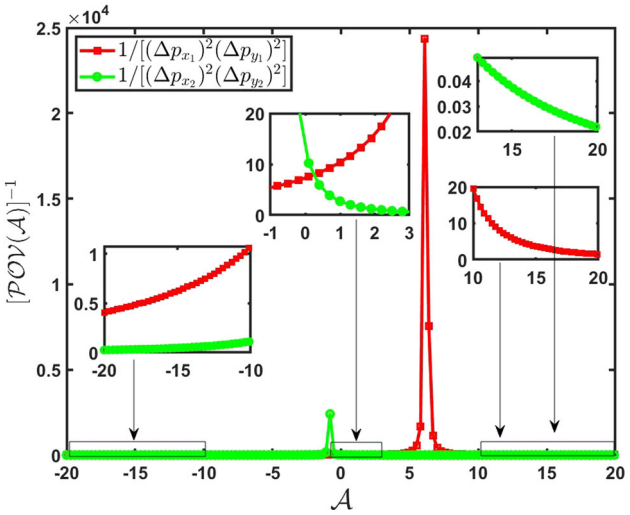

Fig. 2 Plot of reciprocal of $\mathcal{PUV}$ as a function of $\mathcal{A}$. The red and green curve with square and circular marker indices corresponds to the reciprocal of $\mathcal{PUV}$ of Eqs. (89) and (90) (see Appendix 6.2) respectively. The direction of $\vec{\mathcal{B}}$ parallel to $+z$-axis (counterclockwise direction of $\mathcal{A}$) is taken as positive and the negative values of $\mathcal{A}$ on the horizontal axis represents the vector potential curling the field in the opposite direction. The inset plots reveal the system behavior at very large values of $\mathcal{PUV}$. All other parameters same as described above at the start of Sect. 3.1

which is specified by an equation of the following form [20]:

$$L_z^{(k)} = \left(-i\hbar\frac{\partial}{\partial\phi_k} - \alpha\right) \tag{21}$$

where, $k = 1, 2$. The $\mathcal{PUV}$ sets an uncertainty limit on the simultaneous measurement of a specific pair of observables (see Appendix 6.2). In the following sections, the $\mathcal{PUV}$ is plotted as a function of geometric/non-geometric parameters to examine the parameter regimes corresponding to minimal(maximal) uncertainty (entanglement amplification).

3.2 Entanglement amplification via $\vec{\mathcal{B}}$

Figure 2 gives the $\mathcal{PUV}$ between different momentum observables of each subsystem as a function of $\mathcal{A}$. The red (square marker indices) and green (circular marker indices) curves represent the reciprocal of $\mathcal{PUV}(\mathcal{A})$ for Eqs. (89) and (90) respectively. In these curves, an increasing or decreasing $[\mathcal{PUV}(\mathcal{A})]^{-1}$ means a declining or growing product of dispersion, and consequently an amplifying or attenuating entanglement strength, respectively. A sharp peak is evident for a particular value of $\mathcal{A}$ which corresponds to the minimum value of $\mathcal{PUV}$ achievable between these degrees of freedom, which will enhance the entanglement to a maximum. Consequently, the corresponding $\mathcal{A}$ regime would act as an interval of entanglement amplification and an entanglement attenuator away from this interval. This is because the particles are less likely to be effected by the field in these peak regions due to small $\mathcal{A}$, enabling the particles to sustain their quantum correlations. An increasing $\mathcal{A}$ results in entanglement decay due to a stronger influence of the field on particles which leads to a maximum entanglement attenuation near the edges (as seen from the inset plots).

The interval leading to entanglement amplification for $\mathcal{A}$ is as follows:

$$5.2 \leq \mathcal{A}_1 \leq 7.3; \quad -1.4 \leq \mathcal{A}_2 \leq -0.2 \tag{22}$$

where, the subscript of $\mathcal{A}$ represents the particle index. One can see, from Eqs. (89)–(90) (see Appendix 6.2), the $\mathcal{PUV}$ of the i-th particle depends on the angular position of the j-th particle and since $\phi_1 \neq \phi_2$, the peak height of each curve is different.

$\mathcal{B}$ can be obtained from $\mathcal{A}$ by $\mathcal{B} = \frac{\mathcal{A}}{2\pi b}$ and the corresponding $\mathcal{B}$ regions are:

$$0.49277 \leq \mathcal{B}_1 \leq 0.69177; \quad -0.13267 \leq \mathcal{B}_2 \leq -0.01895 \tag{23}$$

The regions defined in Eq. (23) set a limit on the external field strengths for which such a system can sustain its quantum correlations and behaves as an entanglement amplifier. Also, it is observed that entanglement is significantly attenuated around $\mathcal{A} = 0$, from the inset plots. From Eq. (23), it is also evident that $\mathcal{B} \neq 0$ is required for entanglement amplification which highlights the significance of external field in achieving this phenomenon. Thus, for these geometric and entangled systems, it seems possible to control entanglement strength via $\mathcal{B}$, similar to the observation of Ref. [34] for a different setup. It is important to note that although the particles are influenced by the field, they are not directly effected by $\vec{\mathcal{B}}$ but are instead effected by $\vec{\mathcal{A}}$ which also induces a phase shift in the state due to the Aharonov–Bohm effect [17]. This effect is discussed in the context of our problem below.

Phase shift due to the Aharonov–Bohm effect

Figure 3 represents $\mathcal{PUV}$ of Eq. (89) as a function of ϕ_2, corresponding to different $\mathcal{A}$. One can see from Eq. (89) (see Appendix 6.2), the $\mathcal{PUV}$ between momentum degrees of freedom of particle-1 is quadratic in ϕ_2, with all other parameters fixed. Therefore, the curves are parabolic with vertex positioned at the minimum value of $\mathcal{PUV}$, achievable for a given $\mathcal{A}$ (where, $\mathcal{A} = \{0, 1, 2, 3, 4, 5\}$). It is clear from the symmetry of the purple (solid) curve around $\phi_2 = \pi$ (for $\mathcal{A} = 0$), the phase shift is zero in the absence of an external field. The curves corresponding to $\mathcal{A} > 0$, on the other hand, are asymmetric with asymmetry $\propto \mathcal{A}$. Consequently, the dynamics of particle-1 changes and as a result the vertex (at which uncertainty is minimum) of each curve is shifted away from $\phi_2 = \pi$ i.e., the vertex of the curve corresponding to a particular $\mathcal{A}$ lies at $\phi_2 \approx \pi - \mathcal{A}(0.1432\pi)$ with $\Delta\phi_2 \approx \mathcal{A}(0.1432\pi)$ the phase shift; see the points highlighted with red square marker index in the inset plot in Fig. 3. Since, the $\mathcal{PUV}$ is evaluated for Eq. (14), the exponential part

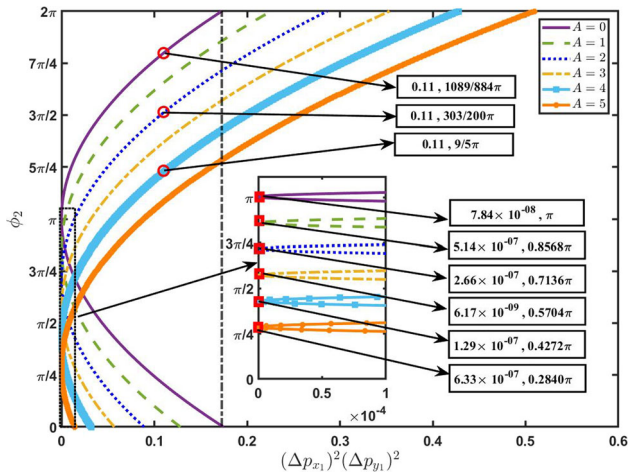

Fig. 3 Line plots representing $\mathcal{POV}$ of Eq. (89) (see Appendix 6.2) as a function of ϕ_2 for different $\vec{\mathcal{A}}$. The graph is plotted for $\alpha = 4.15$ and $\mathcal{A} = \{0, 1, 2, 3, 4, 5\}$. The black vertical line from 0 to 2π exhibits the symmetry of the purple (solid) curve, around $\phi_2 = \pi$, in the absence of external field (i.e., $\mathcal{A} = 0$). All other parameters same as described above at the start of Sect. 3.1. The inset plot reveals the details of the shifted vertex of each curve corresponding to different $\mathcal{A}$

of this equation represents the phase of the composite state with (θ_i, ϕ_i) specifying the particle position on the torus. Hence, any changes in ϕ_2 changes the state of the composite system, which modifies the dynamics of the particles. This is evident from the fact that the phase ϕ_2 corresponding to different $\mathcal{A}$ is different for a fixed value of the $\mathcal{POV}$, as indicated by the red circular marker indices. Moreover, as $\mathcal{A} \to \mathcal{A} + 2$, the phase ϕ_2 shifts by $\Delta\phi_2 = 2\pi/7$. Thus, although the particles are not under direct effect of $\vec{\mathcal{B}}$, the presence of $\vec{\mathcal{A}}$ perturbs the state of the system resulting in phase shift and consequently asymmetric $\mathcal{POV}$. Moreover, it is evident from the points highlighted with red square marker index in the inset plot that the $\mathcal{POV}$ at $\mathcal{A} = 3$ (for which $\Delta\phi_2 \approx 3(0.1432\pi)$) is reduced to minimum in comparison to that observed at $\mathcal{A} = 0$ (for which $\Delta\phi_2 = 0$). This signifies the effect of phase shift due to *Aharonov–Bohm* effect in amplifying entanglement strength.

3.3 Variation of $\mathcal{POV}(x, y)$ under geometric expansion of the torus

Figure 4 provides an illustration of the $\mathcal{POV}$ of Eqs. (62)–(64) (see Appendix 6.2) as a function of radial positions (x, y). From Eq. (16) and the aspect ratio of torus, it is evident that increasing (x, y) gives a torus of increasing radii and hence the background geometry *expands/inflates*, displacing the particles away from $\vec{\mathcal{B}}$ (origin) and vice versa. One must note that the strength of the external field is given by $\mathcal{B} = \mathcal{A}/2\pi b$ and hence $\mathcal{B} \propto 1/b$ which represents position dependence of the field and consequently the system behavior (particle dynamics). Therefore, the $\mathcal{POV}$ is also a function of radial position, denoted as $\mathcal{POV}(x, y)$.

In Fig. 4, the bright yellow and white regions correspond to higher value of the $\mathcal{POV}$ and in this region the system acts as an entanglement attenuator. In the dark brown regime the uncertainty strengths (specified by $\mathcal{POV}$) are much smaller, which means the system can act as an entanglement amplifier with maximal entanglement strength achievable at the minimum uncertainty points highlighted with blue encircled white marker in each plot. It is observed from the *top and bottom left plot* in Fig. 4 that each subsystem responds differently to the *geometric expansion* of the torus. The $\mathcal{POV}$ is higher (lower) for subsystem-1 and lower (higher) for subsystem-2 around origin (edges), leading to a the reciprocal-like behavior. Hence, the uncertainty between the position and momentum observables of both subsystems can be reduced to significantly small strengths if the particles are not in close proximity to each other. The same is true for the y and z-components of position and momentum observables (see *middle* and *right* panel plots). The minimum $\mathcal{POV}$ for $[x_1, p_{x_1}]$ $([x_2, p_{x_2}])$, is achieved at: $(x_1, y_1) = (-0.3493, -0.3860)$ $((x_2, y_2) = (-3.9706, -2.5000))$ with a numerical value of 1.9565×10^{-07} (6.6389×10^{-09}) for subsystem-1 (subsystem-2), same for the conjugate pair $[y_1, p_{y_1}]$ $([y_2, p_{y_2}])$ with the plots flipped due to the particle translation at right angles to x-axis (see *middle panel plots*). For z-component, the $\mathcal{POV}$ of the conjugate pair $[z, p_z]$ for subsystem-1 (subsystem-2) is reduced to minimum i.e., 3.9768×10^{-09} (7.0432×10^{-08}) at $(x_1, y_1) = (-3.8235, -0.5882)$ $((x_2, y_2) = (0.9559, -0.9926))$.

Note, the $\mathcal{POV}$ in traditional HUR with $\hbar = 1$ (since the results in Fig. 4 are plotted by assuming $\hbar = 1$, we use the same for comparison with HUR and GUR) is 0.25 and for GUR the $\mathcal{POV}$ shifts to a smaller value of 0.0625 due to entanglement [11]. However, for this geometric setup, the $\mathcal{POV}$ (specifically at the points highlighted with white encircled blue marker) is reduced significantly below the value obtained in GUR. Hence, constrained entangled particles under the effect of $\vec{\mathcal{B}}$ lead to much smaller uncertainty bounds for the conjugate pair (i.e., $[q, p]$, where $q = (x, y, z)$ and $p = (p_x, p_y, p_z)$) in comparison to GUR.

3.4 $\mathcal{POV}$ as a function of angular position of the particle on torus

Figure 5 represents the color plot of Eq. (91) as a function of angular position (θ_1, ϕ_2). The plots illustrate the influence of poloidal and toridal angle on the $\mathcal{POV}$.

The positive (negative) value of the angle represents the rotation in the counter-clockwise (clockwise) direction. These results highlight how the simultaneous change in the position of both particles effects the $\mathcal{POV}$ and consequently the entanglement strength. *Left plot:* The dark blue regime

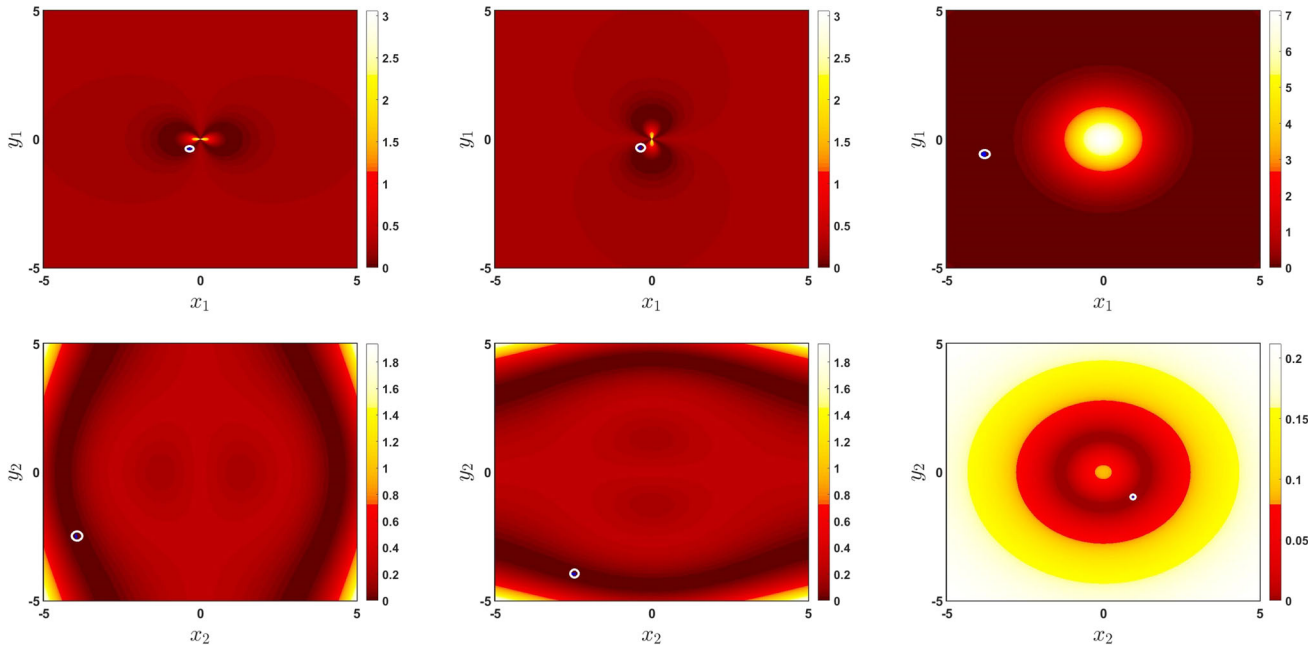

Fig. 4 Upper (lower) panel represents the color plots of $\mathcal{POV}$ between position and momentum observables (see Eqs. (62)–(64) in Appendix 6.2) as a function of (x_1, y_1) $\big((x_2, y_2)\big)$. The left, middle and right plots in upper (lower) panel represents the $\mathcal{POV}$ of $[x, p_x]$, $[y, p_y]$ and $[z, p_z]$ for subsystem-1 (subsystem-2) respectively. In these plots, the points highlighted with white encircled blue marker represent the radial position corresponding to minimum value of the $\mathcal{POV}$. All other parameters same as described above at the start of Sect. 3.1

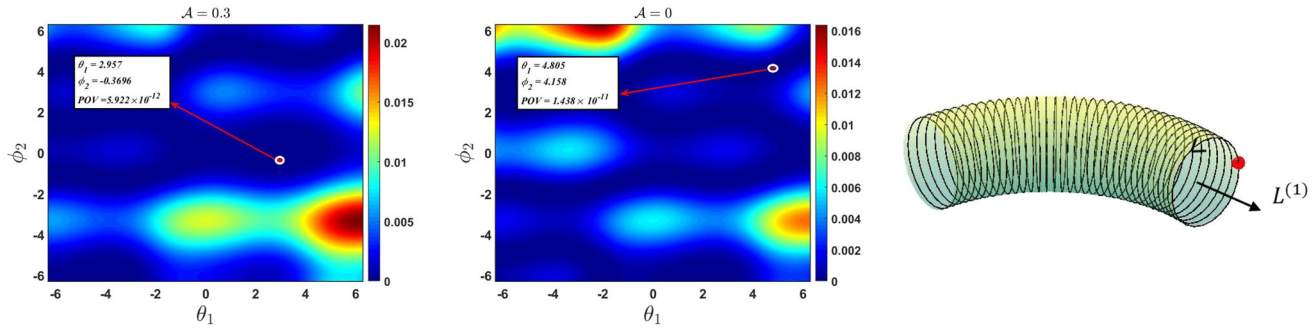

Fig. 5 Left (middle): color plot of $\mathcal{POV}$ of Eq. (91) (see Appendix 6.2) as a function of (θ_1, ϕ_2) corresponding to $\mathcal{A} = 0.3$ ($\mathcal{A} = 0$). The graph is plotted for parameter values: $x_1 = 2, x_2 = 3.1, y_1 = 2.45, y_2 = 0.65$, $k = 2, m = 1, \alpha = 4, \hbar = 1, e = 1, z_1 = 1, z_2 = 1$. The white encircled red marker represents the minimum value of $\mathcal{POV}$. Right: is a schematic representation of the direction of motion of particle-1 and its angular momentum vector ($\mathcal{AMV}$) on the surface of torus (for a better understanding of the orientation of $\mathcal{AMV}$, only a small section of the torus is shown)

represents the points (θ, ϕ) corresponding to lower values of $\mathcal{POV}$, signifying the effect of background geometry on the uncertainty bound specified by the $\mathcal{POV}$. All other regions correspond to relatively higher $\mathcal{POV}$ with dark red regime representing the highest uncertainty. The point highlighted with white encircled red marker illustrates that the $\mathcal{POV}$ is minimum if both particles are traversing the torus in opposite direction. Hence, the minimum (maximal) uncertainty (entanglement strength) is achievable for particle-1 moving in counter-clockwise direction (along increasing poloidal angle) with its angular momentum vector ($\mathcal{AMV}$) $L^{(1)}$ pointing in the direction shown in Fig. 5 and for particle-2 moving in the clockwise direction (along increasing toroidal angle) with its $\mathcal{AMV}$ $L^{(2)}$ pointing antiparallel to $\vec{\mathcal{B}}$. Thus, the $\mathcal{AMV}$ $L^{(1)}$ is at right angles to the $\mathcal{AMV}$ $L^{(2)}$ and since we chose $m = 1$ for both particles, the maximum and minimum value of the integer L, specifying total orbital angular momentum, are obtained by $L_T = 2$ and $L_T = 0$, respectively. Particles are moving in the same direction in the former case and opposite direction in the later case. Since the minimum uncertainty (highlighted in *left plot*) corresponds to particles moving in the opposite direction, we choose $L_T = 0$

for which the total orbital angular momentum is zero, exhibiting the lowest energy (stable) system in analogy with atomic systems. Additionally, one can see from the point highlighted in the *left* and *middle plot*, the $\mathcal{POV}$ provides a more refined uncertainty limit between these degrees of freedom in the presence of $\vec{\mathcal{B}}$, evident from the reduced $\mathcal{POV}$ in the presence of external field.

4 Saturated uncertainty relations and coherent states

In the previous section, we discussed how entanglement strength can be controlled via system parameters and highlighted the parameter strengths corresponding to maximal entanglement amplification. It is also insightful to probe the coherence/decoherence of the entangled state in the presence of $\vec{\mathcal{B}}$, which would be helpful in highlighting the role of external field in maintaining the state coherence. In this section, we test the state coherence by saturating the Robertson inequality associated with angular momentum degrees of freedoms of two different particles. The commutation relations between angular momentum components the particle-k are derived using the Dirac's approach discussed in Sect. 2 and are given below,

$$[\hat{L}_{x_k}, \hat{L}_{y_k}] = i\hbar\hat{L}_z^{(k)} + \frac{i\hbar}{b^2}\left[\hat{y}_k\hat{z}_k(\hat{x}_k\hat{p}_{z_k} + \hat{z}_k\hat{p}_{x_k} - e\hat{x}_k\mathcal{A}_{z_k}) - \hat{x}_k\hat{z}_k(\hat{y}_k\hat{p}_{z_k} + \hat{z}_k\hat{p}_{y_k} - e\hat{y}_k\mathcal{A}_{z_k})\right] \tag{24}$$

where, $k = 1, 2$. We can see (from the second term in above equation) that constraining the particles on a torus in the presence of external fields perturbs the uncertainty relations for angular momentum components. The commutation relation between angular momentum components of two different particles is given by the following equation,

$$\begin{aligned}[\hat{L}_{x_2}, \hat{L}_{y_1}] = \frac{i\hbar}{\sqrt{x_i^2 + y_i^2}}\Bigg[&a\hat{y}_2\hat{z}_1\hat{z}_2 \\ &\times\left((\hat{p}_{x_1} - e\mathcal{A}_{x_1}) + e\mathcal{A}_{x_1}\sqrt{x_i^2 + y_i^2}\right) - \hat{x}_1\hat{y}_2\hat{z}_2\hat{p}_{z_1} \\ &\times\left(\sqrt{x_i^2 + y_i^2} - a\right) + \hat{x}_1\sqrt{x_i^2 + y_i^2}(\hat{p}_{z_1} - e\mathcal{A}_{z_1})\Bigg]\end{aligned} \tag{25}$$

The $\mathcal{POV}$ of Eq. (25) is computed via the Robertson relation and is given as follows,

$$\begin{aligned}(\Delta\hat{L}_{x_2})^2(\Delta\hat{L}_{y_1})^2 \geq{}& \frac{\hbar^2}{\sqrt{x_i^2 + y_i^2}} \\ &\times\Bigg[ay_2z_1z_2\Bigg\{\Bigg(-\frac{m\hbar\sin\phi_1(1+\phi_2)}{(a + b\sin\theta_1)} \\ &-\frac{x_1\hbar\cos\theta_1(1+\theta_2)(a - \sqrt{x_i^2 + y_i^2})}{b^2\sin\theta_1\sqrt{x_i^2 + y_i^2}} \\ &-e\mathcal{A}_{x_1}\Bigg) + e\mathcal{A}_{x_1}\sqrt{x_i^2 + y_i^2}\Bigg\} \\ &+\left(\frac{x_1y_2z_2}{b}\hbar sin\theta_1(1+\theta_2)\left(\sqrt{x_i^2 + y_i^2} - a\right)\right) \\ &-\sqrt{x_i^2 + y_i^2}\left(\frac{x_1}{b}\hbar sin\theta_1(1+\theta_2) - e\mathcal{A}_{z_1}\right)\Bigg]\end{aligned} \tag{26}$$

In Fig. 6, the $\mathcal{POV}$ of Eq. (26) is plotted as a function of (θ_2, ϕ_1) corresponding to different values of the vector potential $\mathcal{A}$. The dark blue (red) regions represent the regions of lower (higher) uncertainty between angular momentum components of different particles. The red encircled white marker represents the saturated limit $\mathcal{SL}$ of Robertson inequality ($\mathcal{SL}$ is the *minimum uncertainty attainable by varying* (θ_2, ϕ_1)). The presence of the terms (θ_2, ϕ_1) in the phasor of the quantum state Eq. (14) implies that a change in θ_2 and ϕ_1 changes the overall quantum state of the system. Therefore, the $\mathcal{SL}$ in each plot represents a higher compatibility of the observables and consequently a quantum state (corresponding to particular (θ_2, ϕ_1)) which is closer to the eigenstate of these observables. It is important to note from the *left* plot that $\mathcal{SL}$ leads to $\theta_2 = \phi_1$ which implies equal phase changes in the state of both particles. Also, since the graph is plotted for $\mathcal{POV}$ of angular momentum components of different particles, the minimum uncertainty region represents the coherence of angular momentum states of these particles, see refs. [35,36]. Additionally, it is evident from both plots that a precise specification of external field strength (i.e., $\mathcal{B} = \mathcal{B}_c = 71.1\text{mT}$) can maintain the coherence of angular momentum states. Note that $\mathcal{B}_c$ represents the coherence range of the external field for which the uncertainty bound is minimized with perfectly correlated phase of the two particles (*left plot*) and for $\mathcal{B} \neq \mathcal{B}_c$ the angular momentum state decoheres (*right plot*).

5 Summary

The interplay between entanglement and uncertainty in the context of constrained systems, specifically for constrained entangled particles subject to a stationary external field $\vec{\mathcal{B}}$, is unknown. In this paper, we address this problem via Dirac's approach and probe for regimes in the parameter space which are useful in amplifying the entanglement strength by reducing the $\mathcal{POV}$. We have also explored the effect of $\vec{\mathcal{B}}$ on $\mathcal{POV}$ in detail. In addition to this, we have shown that $\vec{\mathcal{A}}$ induces a phase shift of $\Delta\phi_2 \approx 2\pi/7$ due to the Aharonov–Bohm effect which alters the system dynamics, resulting asymmetric $\mathcal{POV}$. The effect of background geometry on $\mathcal{POV}$ is also

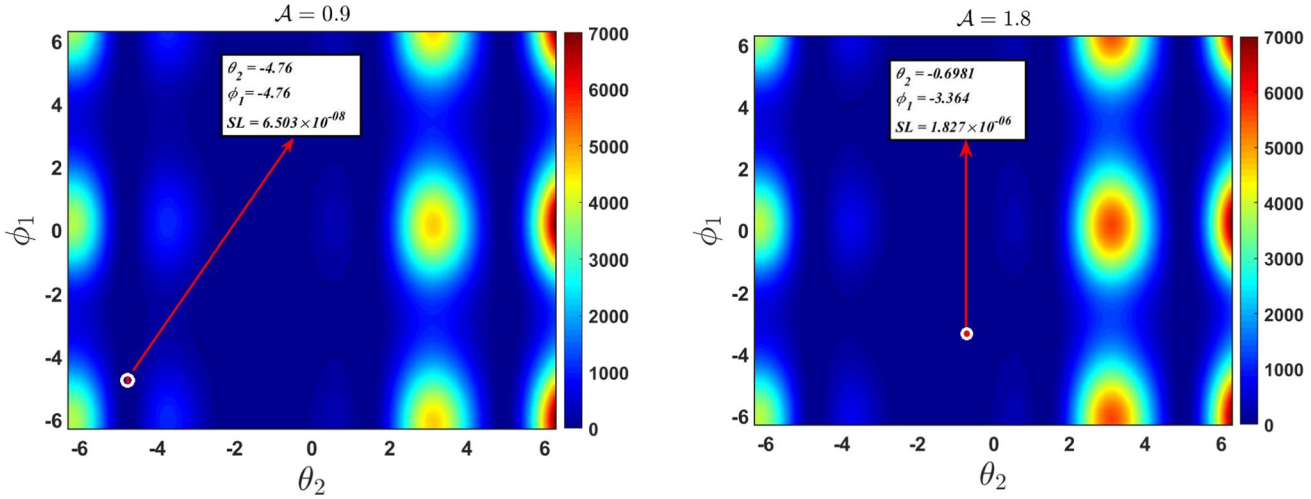

Fig. 6 Color plots of $\mathcal{POV}$ of Eq. (26) as a function of (θ_2, ϕ_1) for different values of $\mathcal{A}$. The red encircled white marker represents the saturated limit $\mathcal{SL}$ of the inequality given in Eq. (26). The graph is plotted for parameter values: $x_1 = 2$, $x_2 = 3.1$, $y_1 = 2.45$, $y_2 = 0.65$, $k = 2$, $m = 1$, $\alpha = 4$, $\hbar = 1$, $e = 1$, $z_1 = 1$, $z_2 = 1$

discussed, which results in perturbations in the entanglement strength for different geometric scenarios, specially the case of an expanding/inflating torus. Also, in view of [11], we note that the lower bound of the Robertson inequality corresponding to the conjugate pair $[q, p]$ can be reduced to significantly smaller values in comparison to the GUR. Furthermore, we have shown that the $\mathcal{POV}$ can be reduced to a minimum provided the $\mathcal{AMV}$ (angular momentum vector) of the two particles point at right angles to each other, resulting in a stable system. Finally, we tested the effect of $\vec{\mathcal{B}}$ on coherence/decoherence of the entangled state by saturating the angular momentum uncertainty relations. We found that at minimum uncertainty (i.e., $\mathcal{SL}$), the angular momentum states exhibit coherence for $\mathcal{B} = \mathcal{B}_c$ and a lack of coherence for $\mathcal{B} \neq \mathcal{B}_c$.

Data Availability Statement My manuscript has no associated data. [Authors' comment: There is no data set associated with our study.].

Code Availability Statement My manuscript has no associated code /software. [Authors' comment: The code generated and analysed during the current study is available from the corresponding author upon reasonable request.].

Funded by SCOAP[3].

6 Appendix

6.1 Dirac brackets

The Dirac brackets between the position and momentum degrees of freedom of each particle are given by the following equations Eqs. (27)–(29).

$$[x_1, p_{x_1}]_D = \left(1 - \frac{x_1^2(a - \sqrt{x_i^2 + y_i^2})^2}{b^2(x_i^2 + y_i^2)}\right);$$

$$[x_2, p_{x_2}]_D = \left(1 - \frac{x_2^2(a - \sqrt{x_i^2 + y_i^2})^2}{b^2(x_i^2 + y_i^2)}\right) \tag{27}$$

$$[y_1, p_{y_1}]_D = \left(1 - \frac{y_1^2(a - \sqrt{x_i^2 + y_i^2})^2}{b^2(x_i^2 + y_i^2)}\right);$$

$$[y_2, p_{y_2}]_D = \left(1 - \frac{y_2^2(a - \sqrt{x_i^2 + y_i^2})^2}{b^2(x_i^2 + y_i^2)}\right) \tag{28}$$

$$[z_1, p_{z_1}]_D = \left(1 - \frac{z_1^2}{b^2}\right);$$

$$[z_2, p_{z_2}]_D = \left(1 - \frac{z_2^2}{b^2}\right) \tag{29}$$

The Dirac brackets Eqs. (30)–(35) represent the momentum generating translation of particle in a direction orthogonal to its position.

$$
\begin{aligned}
[x_1, p_{y_1}]_D &= \frac{-x_1 y_1\left(a-\sqrt{x_i^2+y_i^2}\right)^2}{b^2(x_i^2+y_i^2)};\\
[x_2, p_{y_2}]_D &= \frac{-x_2 y_2\left(a-\sqrt{x_i^2+y_i^2}\right)^2}{b^2(x_i^2+y_i^2)}
\end{aligned}
\tag{30}
$$

$$
\begin{aligned}
[x_1, p_{z_1}]_D &= \frac{x_1 z_1\left(a-\sqrt{x_i^2+y_i^2}\right)}{b^2\sqrt{x_i^2+y_i^2}};\\
[x_2, p_{z_2}]_D &= \frac{x_2 z_2\left(a-\sqrt{x_i^2+y_i^2}\right)}{b^2\sqrt{x_i^2+y_i^2}}
\end{aligned}
\tag{31}
$$

$$
\begin{aligned}
[y_1, p_{x_1}]_D &= \frac{-y_1 x_1\left(\sqrt{x_i^2+y_i^2}-a\right)^2}{b^2(x_i^2+y_i^2)};\\
[y_2, p_{x_2}]_D &= \frac{-y_2 x_2\left(\sqrt{x_i^2+y_i^2}-a\right)^2}{b^2(x_i^2+y_i^2)}
\end{aligned}
\tag{32}
$$

$$
\begin{aligned}
[y_1, p_{z_1}]_D &= \frac{-y_1 z_1\left(\sqrt{x_i^2+y_i^2}-a\right)}{b^2\sqrt{x_i^2+y_i^2}};\\
[y_2, p_{z_2}]_D &= \frac{-y_2 z_2\left(\sqrt{x_i^2+y_i^2}-a\right)}{b^2\sqrt{x_i^2+y_i^2}}
\end{aligned}
\tag{33}
$$

$$
\begin{aligned}
[z_1, p_{x_1}]_D &= \frac{z_1 x_1\left(a-\sqrt{x_i^2+y_i^2}\right)}{b^2\sqrt{x_i^2+y_i^2}};\\
[z_2, p_{x_2}]_D &= \frac{z_1 x_1\left(a-\sqrt{x_i^2+y_i^2}\right)}{b^2\sqrt{x_i^2+y_i^2}}
\end{aligned}
\tag{34}
$$

$$
\begin{aligned}
[z_1, p_{y_1}]_D &= \frac{z_1 y_1\left(a-\sqrt{x_i^2+y_i^2}\right)}{b^2\sqrt{x_i^2+y_i^2}};\\
[z_2, p_{y_2}]_D &= \frac{z_2 y_2\left(a-\sqrt{x_i^2+y_i^2}\right)}{b^2\sqrt{x_i^2+y_i^2}}
\end{aligned}
\tag{35}
$$

The Dirac brackets Eqs. (36)–(44) between the position and momentum degrees of freedom of distinct particles are given below.

$$
\begin{aligned}
[x_1, p_{x_2}]_D &= -\frac{x_1 x_2\left(a-\sqrt{x_i^2+y_i^2}\right)^2}{b^2(x_i^2+y_i^2)};\\
[x_2, p_{x_1}]_D &= -\frac{x_2 x_1\left(a-\sqrt{x_i^2+y_i^2}\right)^2}{b^2(x_i^2+y_i^2)}
\end{aligned}
\tag{36}
$$

$$
\begin{aligned}
[x_1, p_{z_2}]_D &= \frac{x_1 z_2\left(a-\sqrt{x_i^2+y_i^2}\right)}{b^2\sqrt{x_i^2+y_i^2}};\\
[x_2, p_{z_1}]_D &= \frac{x_2 z_1\left(a-\sqrt{x_i^2+y_i^2}\right)}{b^2\sqrt{x_i^2+y_i^2}}
\end{aligned}
\tag{37}
$$

$$
\begin{aligned}
[x_1, p_{y_2}]_D &= -\frac{x_1 y_2\left(a-\sqrt{x_i^2+y_i^2}\right)^2}{b^2(x_i^2+y_i^2)};\\
[x_2, p_{y_1}]_D &= -\frac{x_2 y_1\left(a-\sqrt{x_i^2+y_i^2}\right)^2}{b^2(x_i^2+y_i^2)}
\end{aligned}
\tag{38}
$$

$$
\begin{aligned}
[y_1, p_{y_2}]_D &= -\frac{y_1 y_2\left(a-\sqrt{x_i^2+y_i^2}\right)^2}{b^2(x_i^2+y_i^2)};\\
[y_2, p_{y_1}]_D &= -\frac{y_2 y_1\left(a-\sqrt{x_i^2+y_i^2}\right)^2}{b^2(x_i^2+y_i^2)}
\end{aligned}
\tag{39}
$$

$$
\begin{aligned}
[y_1, p_{x_2}]_D &= -\frac{y_1 x_2\left(a-\sqrt{x_i^2+y_i^2}\right)^2}{b^2(x_i^2+y_i^2)};\\
[y_2, p_{x_1}]_D &= -\frac{y_1 x_2\left(a-\sqrt{x_i^2+y_i^2}\right)^2}{b^2(x_i^2+y_i^2)}
\end{aligned}
\tag{40}
$$

$$
\begin{aligned}
[y_1, p_{z_2}]_D &= \frac{-y_1 z_2\left(\sqrt{x_i^2+y_i^2}-a\right)}{b^2\sqrt{x_i^2+y_i^2}};\\
[y_2, p_{z_1}]_D &= \frac{-y_2 z_1\left(\sqrt{x_i^2+y_i^2}-a\right)}{b^2\sqrt{x_i^2+y_i^2}}
\end{aligned}
\tag{41}
$$

$$[z_1, p_{x_2}]_D = \frac{z_1 x_2\left(a-\sqrt{x_i^2+y_i^2}\right)}{b^2\sqrt{x_i^2+y_i^2}};$$
$$[z_2, p_{x_1}]_D = \frac{z_2 x_1\left(a-\sqrt{x_i^2+y_i^2}\right)}{b^2\sqrt{x_i^2+y_i^2}} \tag{42}$$
$$[z_1, p_{y_2}]_D = \frac{z_1 y_2\left(a-\sqrt{x_i^2+y_i^2}\right)}{b^2\sqrt{x_i^2+y_i^2}};$$
$$[z_2, p_{y_1}]_D = \frac{z_2 y_1\left(a-\sqrt{x_i^2+y_i^2}\right)}{b^2\sqrt{x_i^2+y_i^2}} \tag{43}$$
$$[z_1, p_{z_2}]_D = \frac{-z_1 z_2}{b^2};$$
$$[z_2, p_{z_1}]_D = \frac{-z_1 z_2}{b^2} \tag{44}$$

Equations (45)–(46) provides the Dirac brackets corresponding to translations in momentum space.

$$[x_1, z_1]_D = [x_2, z_2]_D = [x_1, z_2]_D = [x_2, z_1]_D = 0 \tag{45}$$
$$[y_1, z_1]_D = [y_2, z_2]_D = [y_1, z_2]_D = [y_2, z_1]_D = 0 \tag{46}$$

The Dirac brackets representing the translations in position space are listed below in Eqs. (47)–(61).

$$[p_{x_1}, p_{y_1}]_D = -\frac{\left(\sqrt{x_i^2+y_i^2}-a\right)^2\left[x_1(p_{y_1}-e\mathcal{A}_{y_1})-y_1(p_{x_1}-e\mathcal{A}_{x_1})\right]}{b^2(x_i^2+y_i^2)} \tag{47}$$

$$[p_{x_2}, p_{y_2}]_D = -\frac{\left(\sqrt{x_i^2+y_i^2}-a\right)^2\left[x_2(p_{y_2}-e\mathcal{A}_{y_2})-y_2(p_{x_2}-e\mathcal{A}_{x_2})\right]}{b^2(x_i^2+y_i^2)} \tag{48}$$

$$[p_{x_1}, p_{y_2}]_D = -\frac{\left(\sqrt{x_i^2+y_i^2}-a\right)^2\left[x_1(p_{y_2}-e\mathcal{A}_{y_2})-y_2(p_{x_1}-e\mathcal{A}_{x_1})\right]}{b^2(x_i^2+y_i^2)} \tag{49}$$

$$[p_{x_2}, p_{y_1}]_D = -\frac{\left(\sqrt{x_i^2+y_i^2}-a\right)^2\left[x_2(p_{y_1}-e\mathcal{A}_{y_1})-y_1(p_{x_2}-e\mathcal{A}_{x_2})\right]}{b^2(x_i^2+y_i^2)} \tag{50}$$

$$[p_{x_1}, p_{z_1}]_D = \frac{\left(\sqrt{x_i^2+y_i^2}-a\right)\left[x_1(p_{z_1}-e\mathcal{A}_{z_1})+z_1(p_{x_1}-e\mathcal{A}_{x_1})\right]}{b^2\sqrt{x_i^2+y_i^2}} \tag{51}$$

$$[p_{x_2}, p_{z_2}]_D = \frac{\left(\sqrt{x_i^2+y_i^2}-a\right)\left[x_2(p_{z_2}-e\mathcal{A}_{z_2})+z_2(p_{x_2}-e\mathcal{A}_{x_2})\right]}{b^2\sqrt{x_i^2+y_i^2}} \tag{52}$$

$$[p_{x_1}, p_{z_2}]_D = \frac{\left(\sqrt{x_i^2+y_i^2}-a\right)\left[x_1(p_{z_2}-e\mathcal{A}_{z_2})+z_2(p_{x_1}-e\mathcal{A}_{x_1})\right]}{b^2\sqrt{x_i^2+y_i^2}} \tag{53}$$

$$[p_{x_2}, p_{z_1}]_D = \frac{\left(\sqrt{x_i^2+y_i^2}-a\right)\left[x_2(p_{z_1}-e\mathcal{A}_{z_1})+z_1(p_{x_2}-e\mathcal{A}_{x_2})\right]}{b^2\sqrt{x_i^2+y_i^2}} \tag{54}$$

$$[p_{y_1}, p_{z_1}]_D = \frac{\left(\sqrt{x_i^2+y_i^2}-a\right)\left[y_1(p_{z_1}-e\mathcal{A}_{z_1})+z_1(p_{y_1}-e\mathcal{A}_{y_1})\right]}{b^2\sqrt{x_i^2+y_i^2}} \tag{55}$$

$$[p_{y_2}, p_{z_2}]_D = \frac{\left(\sqrt{x_i^2+y_i^2}-a\right)\left[y_2(p_{z_2}-e\mathcal{A}_{z_2})+z_2(p_{y_2}-e\mathcal{A}_{y_2})\right]}{b^2\sqrt{x_i^2+y_i^2}} \tag{56}$$

$$[p_{y_1}, p_{z_2}]_D = \frac{\left(\sqrt{x_i^2+y_i^2}-a\right)\left[y_1(p_{z_2}-e\mathcal{A}_{z_2})+z_2(p_{y_1}-e\mathcal{A}_{y_1})\right]}{b^2\sqrt{x_i^2+y_i^2}} \tag{57}$$

$$[p_{y_2}, p_{z_1}]_D = \frac{\left(\sqrt{x_i^2+y_i^2}-a\right)\left[y_2(p_{z_1}-e\mathcal{A}_{z_1})+z_1(p_{y_2}-e\mathcal{A}_{y_2})\right]}{b^2\sqrt{x_i^2+y_i^2}} \tag{58}$$

$$[p_{x_1}, p_{x_2}]_D = -\frac{\left(\sqrt{x_i^2+y_i^2}-a\right)^2 [x_1(p_{x_2}-e\mathcal{A}_{x_2})-x_2(p_{x_1}-e\mathcal{A}_{x_1})]}{b^2(x_i^2+y_i^2)} \tag{59}$$

$$[p_{y_1}, p_{y_2}]_D = -\frac{\left(\sqrt{x_i^2+y_i^2}-a\right)^2 [y_1(p_{y_2}-e\mathcal{A}_{y_2})-y_2(p_{y_1}-e\mathcal{A}_{y_1})]}{b^2(x_i^2+y_i^2)} \tag{60}$$

$$[p_{z_1}, p_{z_2}]_D = \frac{-z_1(p_{z_2}-e\mathcal{A}_{z_2})+z_2(p_{z_1}-e\mathcal{A}_{z_1})}{b^2} \tag{61}$$

6.2 Product of variance $\mathcal{POV}$

The following inequalities provide the parameter-tunable URs for this geometric setup in the form of $\mathcal{POV}$.

Specifically, the Eqs. (62)–(64) provide the $\mathcal{POV}$ of the conjugate pair for each subsystem.

$$(\Delta\hat{x}_1)^2(\Delta\hat{p}_{x_1})^2 \geq \frac{\hbar^2}{4}\left|1-\frac{x_1^2\left(a-\sqrt{x_i^2+y_i^2}\right)^2}{b^2(x_i^2+y_i^2)}\right|^2;$$

$$(\Delta\hat{x}_2)^2(\Delta\hat{p}_{x_2})^2 \geq \frac{\hbar^2}{4}\left|1-\frac{x_2^2\left(a-\sqrt{x_i^2+y_i^2}\right)^2}{b^2(x_i^2+y_i^2)}\right|^2 \tag{62}$$

$$(\Delta\hat{y}_1)^2(\Delta\hat{p}_{y_1})^2 \geq \frac{\hbar^2}{4}\left|1-\frac{y_1^2\left(a-\sqrt{x_i^2+y_i^2}\right)^2}{b^2(x_i^2+y_i^2)}\right|^2;$$

$$(\Delta\hat{y}_2)^2(\Delta\hat{p}_{y_2})^2 \geq \frac{\hbar^2}{4}\left|1-\frac{y_2^2\left(a-\sqrt{x_i^2+y_i^2}\right)^2}{b^2(x_i^2+y_i^2)}\right|^2 \tag{63}$$

$$(\Delta\hat{z}_1)^2(\Delta\hat{p}_{z_1})^2 \geq \frac{\hbar^2}{4}\left|1-\frac{z_1^2}{b^2}\right|^2;$$

$$(\Delta\hat{z}_2)^2(\Delta\hat{p}_{z_2})^2 \geq \frac{\hbar^2}{4}\left|1-\frac{z_2^2}{b^2}\right|^2 \tag{64}$$

The Eqs. (65)–(84) represents the $\mathcal{POV}$, corresponding to Eqs. (30)–(44), between position and momentum observables of the two subsystems.

$$(\Delta\hat{x}_1)^2(\Delta\hat{p}_{y_1})^2 \geq \frac{\hbar^2}{4}\left|\frac{x_1y_1\left(a-\sqrt{x_i^2+y_i^2}\right)^2}{b^2(x_i^2+y_i^2)}\right|^2;$$

$$(\Delta\hat{x}_2)^2(\Delta\hat{p}_{y_2})^2 \geq \frac{\hbar^2}{4}\left|\frac{x_2y_2\left(a-\sqrt{x_i^2+y_i^2}\right)^2}{b^2(x_i^2+y_i^2)}\right|^2 \tag{65}$$

$$(\Delta\hat{x}_1)^2(\Delta\hat{p}_{z_1})^2 \geq \frac{\hbar^2}{4}\left|\frac{x_1z_1\left(a-\sqrt{x_i^2+y_i^2}\right)}{b^2\sqrt{x_i^2+y_i^2}}\right|^2;$$

$$(\Delta\hat{x}_2)^2(\Delta\hat{p}_{z_2})^2 \geq \frac{\hbar^2}{4}\left|\frac{x_2z_2\left(a-\sqrt{x_i^2+y_i^2}\right)}{b^2\sqrt{x_i^2+y_i^2}}\right|^2 \tag{66}$$

$$(\Delta\hat{y}_1)^2(\Delta\hat{p}_{x_1})^2 \geq \frac{\hbar^2}{4}\left|\frac{y_1x_1\left(\sqrt{x_i^2+y_i^2}-a\right)^2}{b^2(x_i^2+y_i^2)}\right|^2;$$

$$(\Delta\hat{y}_2)^2(\Delta\hat{p}_{x_2})^2 \geq \frac{\hbar^2}{4}\left|\frac{y_2x_2\left(\sqrt{x_i^2+y_i^2}-a\right)^2}{b^2(x_i^2+y_i^2)}\right|^2 \tag{67}$$

$$(\Delta\hat{y}_1)^2(\Delta\hat{p}_{z_1})^2 \geq \frac{\hbar^2}{4}\left|\frac{y_1z_1\left(a-\sqrt{x_i^2+y_i^2}\right)}{b^2(x_i^2+y_i^2)}\right|^2;$$

$$(\Delta\hat{y}_2)^2(\Delta\hat{p}_{z_2})^2 \geq \frac{\hbar^2}{4}\left|\frac{y_2z_2\left(a-\sqrt{x_i^2+y_i^2}\right)}{b^2(x_i^2+y_i^2)}\right|^2 \tag{68}$$

$$(\Delta\hat{z}_1)^2(\Delta\hat{p}_{x_1})^2 \geq \frac{\hbar^2}{4}\left|\frac{z_1x_1\left(a-\sqrt{x_i^2+y_i^2}\right)}{b^2\sqrt{x_i^2+y_i^2}}\right|^2;$$

$$(\Delta\hat{z}_2)^2(\Delta\hat{p}_{x_2})^2 \geq \frac{\hbar^2}{4}\left|\frac{z_2x_2\left(a-\sqrt{x_i^2+y_i^2}\right)}{b^2\sqrt{x_i^2+y_i^2}}\right|^2 \tag{69}$$

$$(\Delta\hat{z}_1)^2(\Delta\hat{p}_{y_1})^2 \geq \frac{\hbar^2}{4}\left|\frac{z_1 y_1\left(a-\sqrt{x_i^2+y_i^2}\right)}{b^2\sqrt{x_i^2+y_i^2}}\right|^2;$$

$$(\Delta\hat{z}_2)^2(\Delta\hat{p}_{y_2})^2 \geq \frac{\hbar^2}{4}\left|\frac{z_2 y_2\left(a-\sqrt{x_i^2+y_i^2}\right)}{b^2\sqrt{x_i^2+y_i^2}}\right|^2 \tag{70}$$

$$(\Delta\hat{x}_1)^2(\Delta\hat{p}_{x_2})^2 \geq \frac{\hbar^2}{4}\left|\frac{x_1 x_2\left(a-\sqrt{x_i^2+y_i^2}\right)^2}{b^2(x_i^2+y_i^2)}\right|^2 \tag{71}$$

$$(\Delta\hat{x}_2)^2(\Delta\hat{p}_{x_1})^2 \geq \frac{\hbar^2}{4}\left|\frac{x_2 x_1\left(a-\sqrt{x_i^2+y_i^2}\right)^2}{b^2(x_i^2+y_i^2)}\right|^2 \tag{72}$$

$$(\Delta\hat{x}_1)^2(\Delta\hat{p}_{z_2})^2 \geq \frac{\hbar^2}{4}\left|\frac{x_1 z_2\left(a-\sqrt{x_i^2+y_i^2}\right)}{b^2\sqrt{x_i^2+y_i^2}}\right|^2 \tag{73}$$

$$(\Delta\hat{x}_2)^2(\Delta\hat{p}_{z_1})^2 \geq \frac{\hbar^2}{4}\left|\frac{x_2 z_1\left(a-\sqrt{x_i^2+y_i^2}\right)}{b^2\sqrt{x_i^2+y_i^2}}\right|^2 \tag{74}$$

$$(\Delta\hat{x}_1)^2(\Delta\hat{p}_{y_2})^2 \geq \frac{\hbar^2}{4}\left|\frac{x_1 y_2\left(a-\sqrt{x_i^2+y_i^2}\right)^2}{b^2(x_i^2+y_i^2)}\right|^2 \tag{75}$$

$$(\Delta\hat{x}_2)^2(\Delta\hat{p}_{y_1})^2 \geq \frac{\hbar^2}{4}\left|\frac{x_2 y_1\left(a-\sqrt{x_i^2+y_i^2}\right)^2}{b^2(x_i^2+y_i^2)}\right|^2 \tag{76}$$

$$(\Delta\hat{y}_1)^2(\Delta\hat{p}_{y_2})^2 \geq \frac{\hbar^2}{4}\left|\frac{y_1 y_2\left(a-\sqrt{x_i^2+y_i^2}\right)^2}{b^2(x_i^2+y_i^2)}\right|^2 \tag{77}$$

$$(\Delta\hat{y}_2)^2(\Delta\hat{p}_{y_1})^2 \geq \frac{\hbar^2}{4}\left|\frac{y_2 y_1\left(a-\sqrt{x_i^2+y_i^2}\right)^2}{b^2(x_i^2+y_i^2)}\right|^2 \tag{78}$$

$$(\Delta\hat{y}_1)^2(\Delta\hat{p}_{x_2})^2 \geq \frac{\hbar^2}{4}\left|\frac{y_1 x_2\left(a-\sqrt{x_i^2+y_i^2}\right)^2}{b^2(x_i^2+y_i^2)}\right|^2 \tag{79}$$

$$(\Delta\hat{y}_2)^2(\Delta\hat{p}_{x_1})^2 \geq \frac{\hbar^2}{4}\left|\frac{y_2 x_1\left(a-\sqrt{x_i^2+y_i^2}\right)^2}{b^2(x_i^2+y_i^2)}\right|^2 \tag{80}$$

$$(\Delta\hat{y}_1)^2(\Delta\hat{p}_{z_2})^2 \geq \frac{\hbar^2}{4}\left|\frac{y_1 z_2\left(\sqrt{x_i^2+y_i^2}-a\right)}{b^2\sqrt{x_i^2+y_i^2}}\right|^2;$$

$$(\Delta\hat{y}_2)^2(\Delta\hat{p}_{z_1})^2 \geq \frac{\hbar^2}{4}\left|\frac{y_2 z_1\left(\sqrt{x_i^2+y_i^2}-a\right)}{b^2\sqrt{x_i^2+y_i^2}}\right|^2 \tag{81}$$

$$(\Delta\hat{z}_1)^2(\Delta\hat{p}_{x_2})^2 \geq \frac{\hbar^2}{4}\left|\frac{z_1 x_2\left(a-\sqrt{x_i^2+y_i^2}\right)}{b^2\sqrt{x_i^2+y_i^2}}\right|^2;$$

$$(\Delta\hat{z}_2)^2(\Delta\hat{p}_{x_1})^2 \geq \frac{\hbar^2}{4}\left|\frac{z_2 x_1\left(a-\sqrt{x_i^2+y_i^2}\right)}{b^2\sqrt{x_i^2+y_i^2}}\right|^2 \tag{82}$$

$$(\Delta\hat{z}_1)^2(\Delta\hat{p}_{y_2})^2 \geq \frac{\hbar^2}{4}\left|\frac{z_1 y_2\left(a-\sqrt{x_i^2+y_i^2}\right)}{b^2\sqrt{x_i^2+y_i^2}}\right|^2;$$

$$(\Delta\hat{z}_2)^2(\Delta\hat{p}_{y_1})^2 \geq \frac{\hbar^2}{4}\left|\frac{z_2 y_1\left(a-\sqrt{x_i^2+y_i^2}\right)}{b^2\sqrt{x_i^2+y_i^2}}\right|^2 \tag{83}$$

$$(\Delta\hat{z}_1)^2(\Delta\hat{p}_{z_2})^2 \geq \frac{\hbar^2}{4}\left|\frac{z_1 z_2}{b^2}\right|^2;$$

$$(\Delta\hat{z}_2)^2(\Delta\hat{p}_{z_1})^2 \geq \frac{\hbar^2}{4}\left|\frac{z_2 z_1}{b^2}\right|^2 \tag{84}$$

The evaluation of $\mathcal{POV}$ for the Eqs. (47)–(61), requires the momentum observables for particles confined to a torus. From Eq. (1), the poloidal and toroidal angle of the particle-k are specified by equations of the following form.

$$\theta_k = cos^{-1}\left(\frac{z_k}{b}\right); \qquad \phi_k = tan^{-1}\left(\frac{y_k}{x_k}\right) \tag{85}$$

where $k = 1, 2$. We know that, for torus, $x_k = x_k(a, b, \theta_k, \phi_k)$. For $k = 1$, the derivative operator is obtained as follows,

$$\begin{aligned}\frac{\partial}{\partial x_1} &= \frac{(a+bsin\theta_1)cos\phi_1}{b} \\ &\times\left(1-\frac{a}{\sqrt{(a+bsin\theta_1)^2+(a+bsin\theta_2)^2}}\right).\left(3\frac{\partial}{\partial a}\right. \\ &\left.+\frac{\partial}{\partial b}\right)+\frac{cos\theta_1(a+bsin\theta_1)cos\phi_1}{b^2} \\ &\times\left(1-\frac{a}{\sqrt{(a+bsin\theta_1)^2+(a+bsin\theta_2)^2}}\right)\frac{1}{sin\theta_1}\frac{\partial}{\partial\theta_1} \\ &-\frac{sin\phi_1}{(a+bsin\theta_1)}\frac{\partial}{\partial\phi_1} \end{aligned} \tag{86}$$

Similarly,

$$\begin{aligned}\frac{\partial}{\partial y_1} &= \frac{(a+bsin\theta_1)sin\phi_1}{b} \\ &\times\left(1-\frac{a}{\sqrt{(a+bsin\theta_1)^2+(a+bsin\theta_2)^2}}\right). \\ &\times\left(3\frac{\partial}{\partial a}+\frac{\partial}{\partial b}\right)+\frac{cos\theta_1(a+bsin\theta_1)sin\phi_1}{b^2} \\ &\times\left(1-\frac{a}{\sqrt{(a+bsin\theta_1)^2+(a+bsin\theta_2)^2}}\right) \\ &\frac{1}{sin\theta_1}\frac{\partial}{\partial\theta_1}\frac{cos\phi_1}{(a+bsin\theta_1)}\frac{\partial}{\partial\phi_1} \end{aligned} \tag{87}$$

$$\frac{\partial}{\partial z_1} = cos\theta_1\left(3\frac{\partial}{\partial a}+\frac{\partial}{\partial b}\right)-\frac{1}{b}sin\theta_1\frac{\partial}{\partial\theta_1} \tag{88}$$

The derivative operators for the second subsystem can be obtained in the same way. The $\mathcal{POV}$ of Eq. (47) is computed using the Robertson relation and is given as follows,

$$(\Delta\hat{p}_{x_1})^2(\Delta\hat{p}_{y_1})^2 \geq \frac{\hbar^2}{4} \times\left|\frac{\left(\sqrt{x_i^2+y_i^2}-a\right)^2[(m\hbar-\alpha)+\phi_2-e(x_1-y_1)\mathcal{A}]}{b^2(x_i^2+y_i^2)}\right|^2 \tag{89}$$

Similarly,

$$(\Delta\hat{p}_{x_2})^2(\Delta\hat{p}_{y_2})^2 \geq \frac{\hbar^2}{4} \times\left|\frac{\left(\sqrt{x_i^2+y_i^2}-a\right)^2[(m\hbar-\alpha)+\phi_1-e(x_2-y_2)\mathcal{A}]}{b^2(x_i^2+y_i^2)}\right|^2 \tag{90}$$

6.2.1 $\mathcal{POV}$ of $[p_{x_i}, p_{y_j}]$

The $\mathcal{POV}$ between the momentum observables of the two distinct particles is given by equations of the following form.

$$\begin{aligned}(\Delta\hat{p}_{x_1})^2(\Delta\hat{p}_{y_2})^2 &\geq \frac{\hbar^2}{4}\left|\frac{\left(\sqrt{x_i^2+y_i^2}-a\right)^2}{b^2(x_i^2+y_i^2)}\right. \\ &\times\left[\frac{x_1y_2\hbar(1+\theta_1)cos\theta_2\left(\sqrt{x_i^2+y_i^2}-a\right)}{b^2sin\theta_2\sqrt{x_i^2+y_i^2}}\right. \\ &+\frac{m\hbar(1+\phi_1)x_1cos\phi_2}{(a+bsin\theta_2)} \\ &-\frac{x_1y_2\hbar(1+\theta_2)cos\theta_1\left(\sqrt{x_i^2+y_i^2}-a\right)}{b^2sin\theta_1\sqrt{x_i^2+y_i^2}} \\ &\left.\left.+\frac{m\hbar(1+\phi_2)y_2sin\phi_1}{(a+bsin\theta_1)}-e\mathcal{A}(x_1-y_2)\right]\right|^2 \end{aligned} \tag{91}$$

$$\begin{aligned}(\Delta\hat{p}_{x_2})^2(\Delta\hat{p}_{y_1})^2 &\geq \frac{\hbar^2}{4}\left|\frac{\left(\sqrt{x_i^2+y_i^2}-a\right)^2}{b^2(x_i^2+y_i^2)}\right. \\ &\times\left[\frac{y_1x_2\hbar(1+\theta_2)cos\theta_1\left(\sqrt{x_i^2+y_i^2}-a\right)}{b^2sin\theta_1\sqrt{x_i^2+y_i^2}}\right. \\ &+\frac{m\hbar(1+\phi_2)x_2cos\phi_1}{(a+bsin\theta_1)} \\ &-\frac{x_2y_1\hbar(1+\theta_1)cos\theta_2\left(\sqrt{x_i^2+y_i^2}-a\right)}{b^2sin\theta_2\sqrt{x_i^2+y_i^2}} \\ &\left.\left.+\frac{m\hbar(1+\phi_1)y_1sin\phi_2}{(a+bsin\theta_2)}-e\mathcal{A}(x_2-y_1)\right]\right|^2 \end{aligned} \tag{92}$$

References

1. A.S. Majumdar, T. Pramanik, Some applications of uncertainty relations in quantum information. Int. J. Quantum Inf. **14**, 1640022 (2016)
2. J.P. Coles, M. Berta, M. Tomamichel, S. Wehner, Entropic uncertainty relations and their applications. Rev. Mod. Phys. **89**, 015002 (2017)
3. J.L. Li, C.F. Qiao, The generalized uncertainty principle. Annalen der Physik **533**, 2000335 (2021)
4. W. Heisenberg, Uber den anschaulichen Inhalt der quantentheoretischen Kinematik und Mechanik. Z. Phys. **43**, 72 (1927)
5. H.P. Robertson, The uncertainty principle. Phys. Rev. **34**, 163 (1929)

6. A. Einstein, B. Podolsky, N. Rosen, Can quantum-mechanical description of physical reality be considered complete? Phys. Rev. **47**, 777 (1935)
7. M. Berta, P.J. Coles, S. Wehner, Entanglement-assisted guessing of complementary measurement outcomes. Phys. Rev. A **90**, 062127 (2014)
8. S. Bagchi, C. Datta, P. Agrawal, Inferred-variance uncertainty relations in the presence of quantum entanglement. Phys. Rev. A **106**, 022203 (2022)
9. H.F. Hofmann, S. Takeuchi, Violation of local uncertainty relations as a signature of entanglement. Phys. Rev. A **68**, 032103 (2003)
10. Y. Akbari-Kourbolagh, M. Azhdargalam, Entanglement criterion for four-partite systems based on local sum uncertainty relations. Eur. Phys. J. Plus **135**, 1–12 (2020)
11. G. Rigolin, Entanglement, identical particles and the uncertainty principle. Commun. Theor. Phys. **66**, 201 (2016)
12. G. Blado, F. Herrera, J. Erwin, Entanglement and the generalized uncertainty principle. Phys. Essays **31**, 397 (2018)
13. A. Ekert, R. Jozsa, Quantum algorithms: entanglement-enhanced information processing. Philos. Trans. Roy. Soc. Lond. Ser. A Math. Phys. Eng. Sci. **356**, 1769 (1998)
14. R. Jozsa, N. Linden, On the role of entanglement in quantum-computational speed-up. Proc. Roy. Soc. A Math. Phys. Eng. Sci. **459**, 2011 (2003)
15. S.A. Nejad, M. Dehghani, M. Monemzadeh, Lagrange multiplier and Wess–Zumino variable as extra dimensions in the torus universe. J. High Energy Phys. **2018**, 1–33 (2018)
16. T.M. Graham, H.J. Bernstein, T.C. Wei, M. Junge, P.G. Kwiat, Superdense teleportation using hyperentangled photons. Nat. Commun. **6**, 7185 (2015)
17. Y. Aharonov, D. Bohm, Significance of electromagnetic potentials in the quantum theory. Phys. Rev. **115**, 485 (1959)
18. V.L. Lyuboshitz, Y.A. Smorodinskii, The Aharonov–Bohm effect in a toroidal solenoid. Sov. J. Exp. Theor. Phys. **48**, 19 (1978)
19. P.A.M. Dirac, Generalized Hamiltonian dynamics. Can. J. Math. **2**, 129 (1950)
20. A. Scardicchio, Classical and quantum dynamics of a particle constrained on a circle. Phys. Lett. A. **300**, 7 (2002)
21. A. Bashir, M.A. Wasay, Constrained dynamics of maximally entangled bipartite system. Eur. Phys. J. C **81**, 303 (2021)
22. H. Kleinert, S.V. Shabanov, Proper Dirac quantization of a free particle on a D-dimensional sphere. Phys. Lett. A. **232**, 327 (1997)
23. D.M. Xun, Q.H. Liu, Can Dirac quantization of constrained systems be fulfilled within the intrinsic geometry? Ann. Phys. **341**, 132 (2014)
24. A. Bashir, M.A. Wasay, A. Al-Mogeeth, Q.H. Liu, Dynamics and uncertainty for maximally entangled bipartite system constrained on a helicoid. Eur. Phys. J. C **82**, 1–12 (2022)
25. X. Da-Mao, O. Tao, T. Rong-Ri, L. Hui-Xuan, Dynamics of the particle on a catenoid and the quantization of the constrained system in the extended space. Acta. Phys. Sin. **64**, 240305 (2015)
26. D.M. Xun, Q.H. Liu, X.M. Zhu, Quantum motion on a torus as a submanifold problem in a generalized Dirac's theory of second-class constraints. Ann. Phys. **338**, 123–133 (2013)
27. D.V. Schroeder, Entanglement isn't just for spin. Am. J. Phys. **85**, 812 (2017)
28. B.J. Dalton, J. Goold, B.M. Garraway, M.D. Reid, Quantum entanglement for systems of identical bosons: I. General features. Phys. Scr. **92**, 023004 (2017)
29. A.G. Agúndez, D. García-Vallejo, E. Freire, Analytical and numerical stability analysis of a toroidal wheel with nonholonomic constraints. Nonlinear Dyn. **112**, 2453–2476 (2024)
30. V. Atanasov, R. Dandoloff, A. Saxena, Torus in a magnetic field: curvature-induced surface states. J. Phys. A Math. Theor. **45**, 105307 (2012)
31. A. Schulze-Halberg, Exact wave functions and energies of a non-relativistic free quantum particle on the surface of a degenerate torus. Mod. Phys. Lett. A. **19**, 1759–1766 (2004)
32. A. Bhattacharjee, M. K. Joshi, S. Karan, J. Leach, A.K. Jha, Propagation-induced revival of entanglement in the angle-OAM bases. Sci. Adv. **8**, eabn7876 (2022)
33. L.C. Venuti, C.D.E. Boschi, M. Roncaglia, Long-distance entanglement in spin systems. Phys. Rev. Lett. **96**, 247206 (2006)
34. Q. Zheng, X.Y. Xie, Q.J. Zhi, Z.Z. Ren, Controllable amplification of entanglement for two qutrits under decoherence. Commun. Theor. Phys. **55**, 569 (2011)
35. M.M. Nieto, L.M. Simmons Jr., Coherent states for general potentials. Phys. Rev. Lett. **41**, 207 (1978)
36. P. Jizba, G. Lambiase, G.G. Luciano, L. Petruzziello, Coherent states for generalized uncertainty relations and their cosmological implications. J. Phys. Conf. Ser. **2533**(1), 012043 (2023)